# First-principles calculations on the origin of ferromagnetism in transition-metal doped Ge

Hikari Shinya*
*Graduate School of Engineering, Yokohama National University, Yokohama, Kanagawa, 240-8501, Japan*
*and Center for Spintronics Research Network, Osaka University, Toyonaka, Osaka 560-8531, Japan*

Tetsuya Fukushima
*Institute for NanoScience Design, Osaka University, Toyonaka, Osaka 560-8531, Japan*
*and Institute for Datability Science, Osaka University, Suita, Osaka 565-0871, Japan*

Akira Masago
*Center for Spintronics Research Network, Osaka University, Toyonaka, Osaka 560-8531, Japan*

Kazunori Sato
*Graduate School of Engineering, Osaka University, Suita, Osaka 565-0871, Japan*

Hiroshi Katayama-Yoshida
*Center for Spintronics Research Network, The University of Tokyo, Bunkyo-ku, Tokyo 113-8656, Japan*
(Received 18 July 2017; published 12 September 2017)

Many researchers have shown an interest in Ge-based dilute magnetic semiconductors (DMSs) due to potential advantages for semiconductor spintronics applications. There has been great discussion about mechanisms of experimentally observed ferromagnetism in (Ge,Fe) and (Ge,Mn). We investigate the electronic structures, structural stabilities, magnetic exchange coupling constants, and Curie temperature of Ge-based DMSs, and clarify origins of the ferromagnetism, on the basis of density functional theory calculations. In both the (Ge,Fe) and (Ge,Mn) cases, the inhomogeneous distribution of the magnetic impurities plays an important role to determine the magnetic states; however, physical mechanisms of the ferromagnetism in these two materials are completely different. By the spinodal nanodecomposition, the Fe impurities in Ge gather together with keeping the diamond structure, so that the number of the first-nearest-neighbor Fe pairs with strong ferromagnetic interaction increases. Therefore, the Curie temperature drastically increases with the progress of the annealing. Our cluster expansion method clearly reveals that the other ordered compounds with different crystal structures such as $Ge_3Mn_5$ and $Ge_8Mn_{11}$ are easily generated in the (Ge,Mn) system. The estimated Curie temperature of $Ge_3Mn_5$ is in agreement with the observed Curie temperature in experiments. It should be considered that the precipitation of the ferromagnetic $Ge_3Mn_5$ clusters is an origin of high Curie temperature in (Ge,Mn).

DOI: 10.1103/PhysRevB.96.104415

## I. INTRODUCTION

Utilizing spin degrees of freedom of electrons in semiconductors (semiconductor spintronics) opens the way to new functionalities in next-generation electronics, such as high-integration, high-speed nonvolatile memory, integrated-type magneto-optical devices, and quantum computers [1,2]. Dilute magnetic semiconductors (DMSs), in which magnetic impurities are doped to semiconductor hosts, have been expected as one of candidates to realize the semiconductor spintronics [3–6]. So far, III-V-type (InAs, GaN, GaAs, etc.) and II-VI-type (CdTe, ZnO, ZnTe, etc.) semiconductors have been mainly employed for the DMS host materials. In particular, (Ga,Mn)As is a prototype DMS, and has been well studied in terms of physics and industrial applications.

For practical applications, one needs to synthesize DMSs with Curie temperature ($T_C$) much higher than the room temperature (∼300 K). Over the past few years, many efforts have been devoted to the realization of the high-$T_C$ DMS. Actually, there have been several experimental reports for the room-temperature ferromagnetism [7–14]. However, the majority of these have been observed in low magnetic impurity regions, contradicting with a theoretical result, where ferromagnetic transitions do not occur due to the magnetic percolation effect [15,16]. Sato and Katayama-Yoshida pointed out that such strange ferromagnetism is due to the inhomogeneous distribution of magnetic impurities by the spinodal nanodecomposition, i.e., the blocking phenomenon caused by nanocolumn structures is strongly related to the ferromagnetism [17,18]. The spinodal nanodecomposition is nowadays widely recognized to be an important factor for understanding ferromagnetism in DMSs [19].

Recently, the IV-type semiconductor Ge has attracted much attention as the host material for the following two reasons: (i) Ge possesses higher mobility than that of Si; therefore, it has the possibility of the realization of high-speed and low-power consumption LSI systems; (ii) Ge has a good compatibility with the Si-CMOS technology. Jamet [20] and Devillers [21] observed a ferromagnetic state with high $T_C$ (>400 K) in (Ge,Mn) epitaxial layer, and carefully investigated the Mn morphology and composition by using the transmission electron microscopy (TEM) and electron energy loss spectroscopy (EELS) techniques. They found that the distribution of the

*shinya-hikari-sb@ynu.ac.jp

 

Mn atoms is not spatially homogeneous, and in particular the Mn atoms form quasi-one-dimensional nanocolumns along the crystal growth direction. Such nanocolumns are intimately related to the appearance of the high-$T_C$ ferromagnetism in (Ge,Mn). Wakabayashi *et al.* demonstrated the enhancement of $T_C$ and nonuniformity of the Fe atoms in (Ge,Fe) by an experimental annealing technique [22]. According to their study, $T_C$ of $Ge_{0.895}Fe_{0.105}$ is improved and reaches 210 K by the annealing below 600 °C, while the $T_C$ increases up to the room temperature when the annealing temperature is 600 °C; however, stacking fault and twins happen. They also investigated the local magnetic properties of (Ge,Fe) by the x-ray absorption spectroscopy (XAS) and soft x-ray magnetic circular dichroism (XMCD), and suggested that even at room temperature the local ferromagnetic region is still kept, and then the expansion of this region progresses with decreasing temperature, resulting in the ferromagnetic phase transition [23,24]. For both the (Ge,Mn) and (Ge,Fe) cases, the inhomogeneous distributions of the Mn and Fe atoms play an important role for the magnetic properties.

In this paper, we perform the density functional theory calculations [25,26] for transition-metal (TM) impurities doped Ge by using the Korringa-Kohn-Rostoker (KKR) Green's function method with the coherent potential approximation (CPA) [27–30], to theoretically shed light on the ferromagnetic mechanisms of the Ge-based DMS systems. Our calculations show that, when the Mn impurities are randomly distributed in Ge, antiferromagnetic interactions work between the doped Mn pairs. Secondary phases generated by Ge and Mn are potentially associated with the experimentally observed ferromagnetism in (Ge,Mn) [31]. For the (Ge,Fe) system, the electronic structure and density of states calculated by the KKR-CPA combined with the variational pseudo-self-interaction correction (VP-SIC) method [32] are reasonably consistent with the results of experimentally observed x-ray angle-resolved photoemission spectroscopy (SX-ARPES) [23]. Although the Fe atoms couple ferromagnetically with each other, the interaction range cased by the double exchange mechanism is rather short. Due to the increase of the first-nearest-neighbor Fe pairs with strong ferromagnetic interaction by the spinodal nanodecomposition, the high-$T_C$ states are stabilized.

The outline of this paper is as follows. In Sec. II, our computational methods and calculation conditions for the electronic structure, magnetic exchange coupling constants, and $T_C$ are explained. In Sec. III, the chemical trends of the electronic structure and magnetism of the TM-doped Ge are given, and then we focus on how the inhomogeneous Mn and Fe distributions affect the magnetic states of (Ge,Mn) and (Ge,Fe). Section IV is devoted to the summary in this paper.

## II. COMPUTATIONAL METHODS

In this paper, the electronic structures and magnetic properties of the TM impurities doped Ge are mainly calculated by MACHIKANEYAMA2002 program package [33], where the KKR Green's function method [27,28] is implemented within the density functional theory [25,26]. The randomness of the doped TM impurities in the Ge host is treated by the coherent potential approximation (CPA) in which the multiple scattering effect is replaced by an effective medium potential [29,30]. It is well known that the local density approximation (LDA) fails to describe localized $d$ states in transition metal elements. To overcome this LDA error, we use the VP-SIC method proposed by Filippetti *et al.* [32], when comparing with experimental data by SX-ARPES. The PSIC method has already applied to several DMS systems, such as (Ga,Mn)N, (Ga,Mn)As, and (Zn,TM)O, and gives reasonably consistent results with experimental data [34,35]. During the KKR calculations, the lattice constant of host Ge is fixed to the experimental lattice constant: $a = 5.651$ Å, and TM atoms are introduced in the substitutional position of Ge atoms. We choose 868 $k$-sampling points in the first irreducible Brillouin zone. The relativistic effects are considered by the scalar relativistic approximation. For exploring possible ordered compounds of the Mn and Ge atoms, we also use the Alloy Theoretical Automated Toolkit (ATAT) program package [36–38], in which a cluster-expansion-based structure searching algorithm is implemented, and Vienna *ab initio* simulation package (VASP) [39–41], on the basis of the projector augmented wave (PAW) method [42]. In the VASP calculations, we use Monkhorst-Pack [43] $k$-point meshes and set the plane wave cutoff energy to 400 eV. During structural optimization, the threshold of the atomic forces is set to 0.01 eV/Å.

We calculate the Heisenberg exchange coupling constants between the TM impurities ($J_{ij}$) to quantitatively discuss the magnetic interactions, on the basis of the Liechtenstein's formula [44]. In the Liechtenstein's formula, according to the magnetic force theorem [45], we consider a perturbation by infinitesimal rotations of magnetic moments. Mapping the energy change due to the perturbation to the effective classical Heisenberg model, one can calculate $J_{ij}$ as follows:

$$J_{ij} = -\frac{1}{4\pi}\mathrm{Im}\int_{E_B}^{E_F} dE\ \mathrm{Tr}_L\{\Delta_i T_\uparrow^{ij}\Delta_j T_\downarrow^{ji}\}. \qquad (1)$$

Here $\Delta_i$ is the difference of the atomic $t$ matrix between the spin-up and spin-down states, i.e., $\Delta_i = t_{i\uparrow}^{-1} - t_{i\downarrow}^{-1}$. $T_{\uparrow(\downarrow)}^{ij}$ is the off-diagonal scattering path operator between site $i$ and $j$ for the spin-up (down) state, which can be easily calculated in the KKR formalism. $\mathrm{Tr}_L$ denotes the trace over the orbital variables ($l$ and $m$). We perform the energy integration from the valence band bottom ($E_B$) to the Fermi energy ($E_F$). $T_C$ of the TM-doped Ge can be calculated by the results of $J_{ij}$ and the classical Heisenberg model. Here, we employ the random phase approximation (RPA), which is based on the Tyablikov decoupling method for magnon Green's function [46,47]. The RPA method can take the magnetic percolation effect into consideration. Note that the mean-field approximation, which neglects the magnetic percolation effect strongly overestimates $T_C$ for disordered systems [15,16]. In RPA, $T_C^{RPA}$ can be expressed by

$$k_B T_C^{RPA} = \frac{2}{3}\left(\frac{1}{N}\sum_r \frac{1}{E_r}\right)^{-1}, \qquad (2)$$

where $N$ is the number of the TM impurities in the considered supercell and $E_r$ is the eigenvalue of the Hamiltonian matrix $H$, which is defined by $H_{ij} = \delta_{ij}(\sum_{n=1}^{N} J_{in}) - J_{ij}$. The $J_{ij}$ interactions up to 15 shells are included in our simulations.

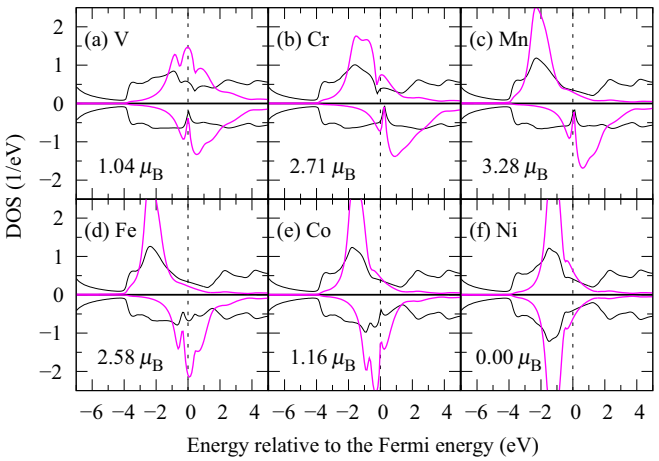


FIG. 1. DOSs of (a) (Ge,V), (b) (Ge,Cr), (c) (Ge,Mn), (d) (Ge,Fe), (e) (Ge,Co), and (f) (Ge,Ni) calculated by LDA. The total and partial $d$ DOSs are shown in black and magenta lines, respectively. The concentration of the TM impurities are 10%. The horizontal axis corresponds to energy relative to the Fermi level. The local magnetic moments for the doped TM atoms are also indicated in the figure.

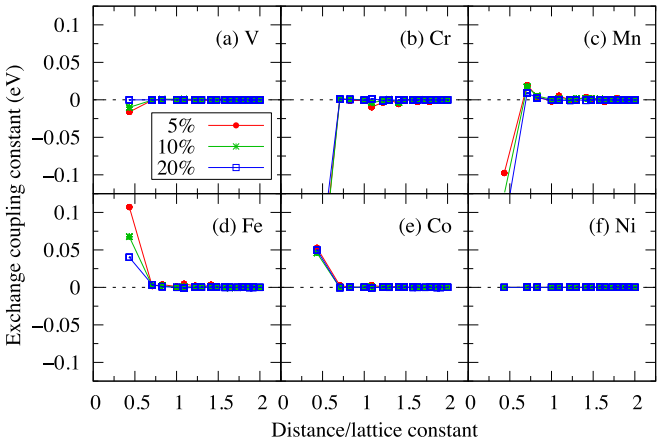


FIG. 2. $J_{ij}$ values between (a) V-V, (b) Cr-Cr, (c) Mn-Mn, (d) Fe-Fe, (e) Co-Co, and (f) Ni-Ni pairs in Ge. The horizontal axis corresponds to the distance between the doped TM atoms. The TM impurity concentrations are 5% (red line), 10% (green line), and 20% (blue line). The positive and negative values mean ferromagnetic and antiferromagnetic interactions, respectively.

Chemical pair interactions ($V_{ij}$) between the TM impurities are also calculated, based on the generalized perturbation method proposed by Ducastelle and Gautier [48]. In the generalized perturbation method, the configuration-dependent energy, which is deviated from a completely disordered CPA system, is expanded by concentration fluctuation. For a binary alloy AB, in the lowest order of the perturbation, $V_{ij}$ is given by

$$V_{ij} = -\frac{1}{\pi}\mathrm{Im}\int_{E_B}^{E_F} dE\ \mathrm{Tr}_L\{\Delta T^{ij}\Delta T^{ji}\}, \qquad (3)$$

where $\Delta = t_A^{-1} - t_B^{-1}$. Combining the above approaches, we perform multiscale (scale-bridging) simulations for the Ge-based DMS systems. So far, this multiscale simulation method has been successful in investigating the electronic structure and magnetic properties in DMS systems. For example, for (Zn,Cr)Te and (Ga,Mn)As, the estimated $T_C$ values are quantitatively in good agreement with experimentally observed results. Readers can see the details and effectiveness of our calculation method in Refs. [5] and [19].

## III. RESULTS

### A. Chemical trend

#### 1. Electronic structure

We start with discussion of the electronic structures of the Ge-based DMS. Figure 1 shows the total and partial densities of states (DOSs) of [Figs. 1(a)] V, [1(b)] Cr, [1(c)] Mn, [1(d)] Fe, [1(e)] Co, and [1(f)] Ni 10% doped Ge calculated by LDA. For each system, the upper and lower parts correspond to the majority and minority spin states, respectively. Total DOSs per the unit cell are described by the black lines and the partial $d$ DOSs per the atom are plotted by the magenta lines. In the semiconductor Ge, the $4s$ and $4p$ form the $sp^3$ hybrid orbitals, so that the valence bands are formed by the bonding $sp^3$ orbitals and the main part of the conduction bands are the $sp^3$ antibonding orbitals, resulting in the stabilization of the tetrahedral diamond structure. In the Ge-based DMSs, the TM atoms are tetrahedrally surrounded by the Ge atoms; therefore, the fivefold TM $d$ states split into the $t_2$ and $e$ states by the crystal field splitting. The competition between the crystal field splitting and exchange splitting determines the spin states (i.e., high-spin or low-spin state). The $d$ orbitals of the doped V and Cr atoms are rather spatially extended, compared to the cases of the late transition-metals (Mn, Fe, Co, and Ni), and hybridize well with the host Ge $p$ states. This hybridization leads to the smeared partial $d$ DOSs in the majority spin states and the stabilization of the low spin state, in which the crystal field splitting is larger than the exchange splitting, as shown in Figs. 1(a) and 1(b). On the other hand, in the [Figs. 1(c)] Mn- and [1(d)] Fe-doped cases, due to the localized $d$ orbitals and weak crystal field splitting, the high spin states are realized. The PDOSs of Mn, Fe, and Co in the majority spin states are almost the same, while those in the minority spin states gradually become larger with increasing the number of occupied electrons by the weak exchange splitting. In Ni-doped Ge, there is no exchange splitting between the majority and minority spin states, so that a finite magnetic moment cannot be expected.

#### 2. Magnetic exchange coupling constant

Generally, DOSs and band structures can not give any quantitative information about the magnetic interactions in materials. For discussing the magnetic interactions in Ge-based DMSs quantitatively, one needs to calculate $J_{ij}$ between the doped TM impurities. Figure 2 shows the $J_{ij}$ values between the magnetic impurities calculated by the Liechtenstein's formula. The positive (negative) $J_{ij}$ values in the figure mean the ferromagnetic (antiferromagnetic) interactions, and the horizontal axis corresponds to the distance between the TM pairs. According to our calculations, the ferromagnetic interactions work in the Fe- and Co-doped Ge systems, while the antiferromagnetic couplings are realized for the V-V and Cr-Cr pairs. The ferromagnetic interactions of the Fe-Fe

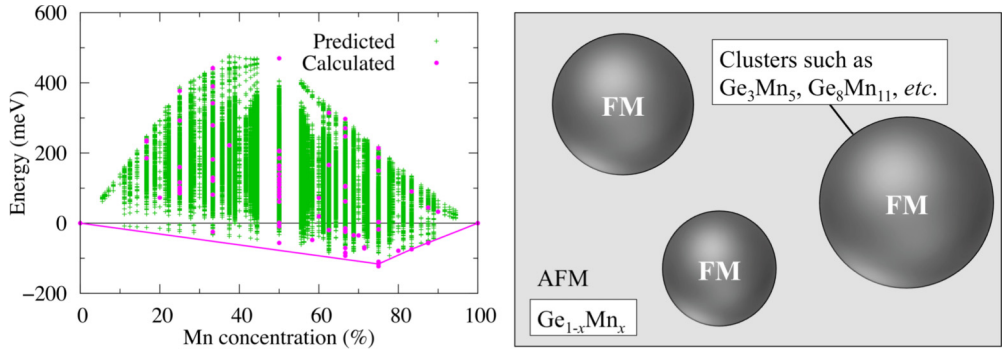


FIG. 3. (Left) Formation energies of the (Ge,Mn) system by the cluster expansion method. The magenta and green points indicate the DFT calculated and predicted energies, respectively. The horizontal axis is the Mn concentration. The ground states are connected by the magenta lines. (Right) Schematic figure of the ferromagnetic precipitations ($Ge_3Mn_5$, $Ge_8Mn_{11}$, etc.) in the antiferromagnetic (Ge,Mn) host.

and Co-Co pairs are quite short ranged; the first-nearest-neighbor interactions are significant, and the other nearest-neighbor interactions are very small. Such tendency of the ferromagnetic interaction can be understood from their electronic structures. Sato *et al.* proposed that the ferromagnetic features in DMS systems are dominated by the two mechanisms, i.e., the double exchange interaction and *p-d* exchange interaction [15]. The former becomes prominent when the partially occupied TM-*d* states appears in the band gap. The hopping of the TM-*d* electrons reduces the kinetic energy such that the ferromagnetic state is stable. Interactions caused by the double exchange mechanism are short ranged, reflecting the fact that an impurity wave function in a band gap decays exponentially. In the opposite situation, where the TM-*d* states are located on an energetically deeper region compared to the host valence bands, the *p-d* exchange interaction plays an important role. The polarized *p* holes move around, aligning the spins of the localized TM-*d* electrons in parallel; therefore, long-ranged ferromagnetic interaction is realized. Thus, the relative position between the TM-*d* and host *p* states determines the dominant ferromagnetic mechanism. Note that the above classification is based on the two extreme situations, and ferromagnetism in real DMS systems should be stabilized by the combination of the two mechanisms. As shown in Figs. 1(d) and 1(e), in the Fe- and Co-doped Ge, the main character on the Fermi level is TM *d* states, so that it should be considered that the dominant ferromagnetic mechanism is the double exchange interaction rather than the *p-d* exchange interaction. It is worthwhile to compare the ferromagnetic feature of (Ge,Fe), where the interaction is the most strong among the Ge-based DMS, with a general ferromagnetic DMS system (Ga,Mn)As. (Ga,Mn)As has a long-ranged ferromagnetic interaction, which extends farther than the 20th-nearest-neighbor Mn-Mn pairs, due to the *p-d* exchange mechanism [15]. $T_C$ of (Ga,Mn)As nowadays reaches around 200 K [49,50]. Since the ferromagnetic state in (Ge,Fe) is stabilized by the short-ranged double exchange mechanism, it is considered that the realization of high $T_C$ above $T_C$ of (Ga,Mn)As is so difficult, if the distribution of the Fe atoms is random.

### B. Origin of ferromagnetism in (Ge,Mn)

As mentioned in Sec. I, the high-$T_C$ ferromagnetism above the room temperature was experimentally observed in epitaxially grown (Ge,Mn) [20,21]. However, the $J_{ij}$ values calculated by the Liechtenstein's formula clearly show that antiferromagnetic interactions are ascendant for the Mn-Mn pairs in Ge. In this section, we focus on an origin of the experimentally observed high-$T_C$ ferromagnetism. Our CPA calculation is based on the assumption that the TM impurities are randomly distributed in Ge hosts, i.e., effects of other ordered phases and secondary phases on the magnetic properties are not taken into consideration. In order to evaluate the phase stability of (Ge,Mn), we perform the cluster expansion method. Figure 3 shows the results, in which the vertical (horizontal) axis is the formation enthalpy (Mn concentration). Here, the formation enthalpy is defined as

$$\Delta H_f = E(\mathrm{Ge}_{1-x}\mathrm{Mn}_x) - (1-x)E(\mathrm{Ge}) - xE(\mathrm{Mn}), \quad (4)$$

where $x$ is concentration of Mn atom, and $E(\mathrm{Ge}_{1-x}\mathrm{Mn}_x)$, $E(\mathrm{Ge})$, and $E(\mathrm{Mn})$ are the total energies of $\mathrm{Ge}_{1-x}\mathrm{Mn}_x$ alloy, pure Ge atom, and pure Mn atom. In the figure, the magenta and green circles denote calculated structures and predicted structures by the cluster expansion method, respectively. The structures on the magenta lines are ground-state structures. Several ground-state structures can be found in the Mn-rich regions. This means that the Mn impurities are not distributed randomly, but ordered compounds and secondary phases, whose crystal structures are no longer the diamond structure, are generated. The cluster expansion method suggests the possibility that the ordered compounds, such as $Ge_3Mn_5$ and $Ge_8Mn_{11}$, precipitate in the antiferromagnetic (Ge,Mn) hosts, as schematically shown in Fig. 3. For example, the ferromagnetic state is intrinsically stable in $Ge_3Mn_5$. Figure 4 shows the crystal structure of $Ge_3Mn_5$ with the $P6_3/mcm$ symmetry ($a = 7.184$ Å, $c = 5.053$ Å, and $\gamma = 120^\circ$) [51], and the calculated $J_{ij}$ values for the first-, second-, and third-nearest-neighbor Mn-Mn pairs.

$T_C$ of $Ge_3Mn_5$ is estimated to be 315 K by the mean-field approximation and the calculated $J_{ij}$ values, i.e., $k_B T_C = \frac{2}{3}\sum_j J_{0j}$. The calculated $T_C$ is quite consistent with the experimental observed value of a sample grown at a high temperature [20,21]. Note that the mean-field approximation fails for disordered systems due to the lack of the percolation effect, but gives reasonable results for ordered systems. Consequently, it should be considered that the precipitation

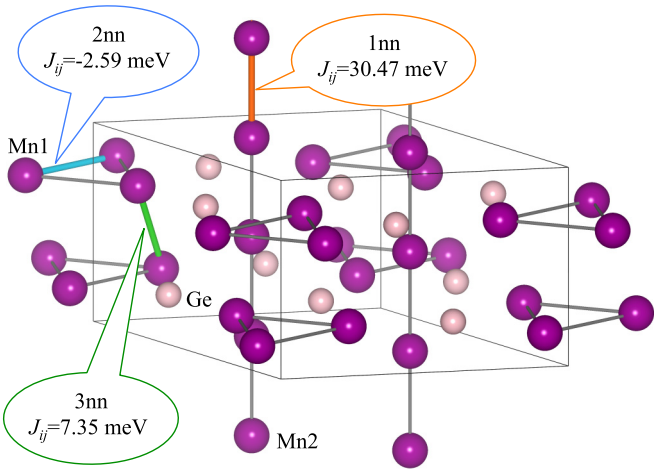


FIG. 4. Crystal structure of $Ge_3Mn_5$ with the $P6_3/mcm$ symmetry. The purple and pink spheres indicate and Mn and Ge atoms, respectively. $J_{ij}$ values of the Mn-Mn pairs for the first, second, and third nearest neighbors (1 nn, 2 nn, and 3 nn) are shown.

of the ferromagnetic $Ge_3Mn_5$ clusters is an origin of the high $T_C$ in the (Ge,Mn) system.

### C. Spinodal nanodecomposition in (Ge,Fe)

(Ge,Fe) has gotten a lot of interest recently due to the novel magnetic properties and relatively high $T_C$. In this section, we look at the electronic structure and magnetic property of (Ge,Fe) in detail. Figure 5 shows total and partial DOSs of (Ge,Fe) calculated by [Fig. 5(a)] LDA and [Fig. 5(b)] VP-SIC methods. Compared to the LDA calculations, the Fe-$d$ states are more localized and pushed down to energetically deeper region in the VP-SIC method. This is due to the fact that, in the LDA scheme, the self-interaction terms in the Hartree and exchange parts are not canceled, leading to the stabilization of a delocalized state [52]. The position of the Fe-$d$ states [indicated by the black arrow in Fig. 5(b)] is in good agreement with the spectrum observed by the SX-ARPES measurement [23]. Therefore, it can be expected

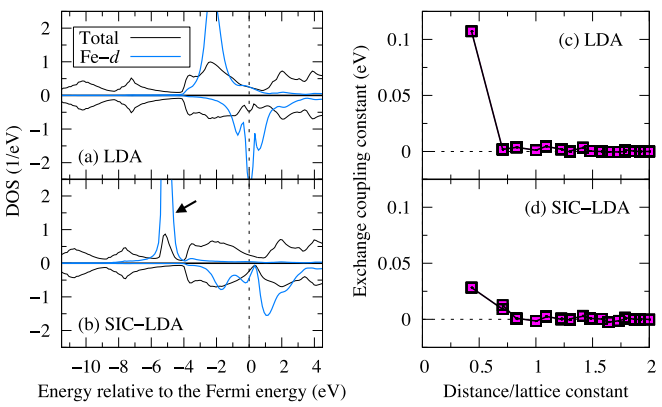


FIG. 5. (Left) Total and partial DOSs of GeFe calculated by (a) LDA and (b) VP-SIC methods. (Right) $J_{ij}$ values of ($Ge_{0.95}$,$Fe_{0.05}$) calculated by the Liechtenstein's formula with (c) LDA and (d) VP-SIC methods.

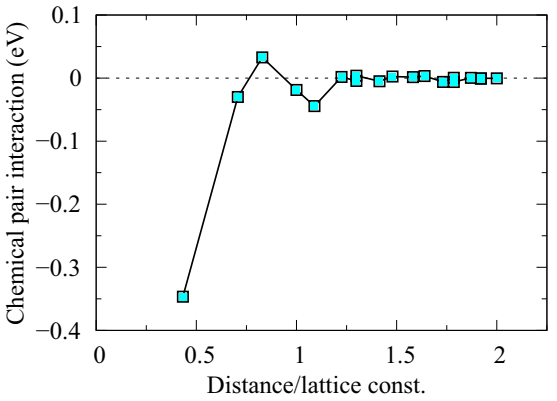


FIG. 6. Chemical pair interaction ($V_{ij}$) of ($Ge_{0.895}$,$Fe_{0.105}$) as a function of distance between the Fe atoms. The positive and negative $V_{ij}$ correspond to repulsive and attractive interactions, respectively.

that the VP-SIC method describes the localized Fe-$d$ states in Ge well. Reflecting the more localized orbitals by the VP-SIC method, the ferromagnetic interaction becomes weak and short ranged compared to the LDA case, as shown in Figs. 5(c) and 5(d). Note that the comprehensive comparison with the LDA for the all dopants can be seen in the Supplemental Material [53]. In the experiments for $Ge_{0.895}Fe_{0.105}$, relatively high-$T_C$ phases (210 $\sim$ 300 K) were observed [22,24]. Considering the short-ranged ferromagnetic interaction and the low Fe concentration, one cannot expect that such high-$T_C$ ferromagnetism is realized due to the magnetic percolation effect. For example, when assuming only the first-nearest-neighbor interaction, the percolation threshold is around 0.43. In actual materials, by longer-ranged interactions, the percolation threshold increases. As in the case of (Ge,Mn), inhomogeneity of the Fe atoms or structural instability might be considered as a key rule of the high $T_C$ in (Ge,Fe).

Figure 6 shows the $V_{ij}$ values between the Fe pairs in Ge calculated by the generalized perturbation method [see Eq. (3)]. An alternative definition of $V_{ij}$ is given by $V_{ij} = V_{ij}^{\mathrm{Fe-Fe}} + V_{ij}^{\mathrm{Ge-Ge}} - 2V_{ij}^{\mathrm{Fe-Ge}}$, where $V_{ij}^{\mathrm{A-B}}$ is the potential energy when A and B atoms are located on the site of $i$ and $j$. A positive (negative) $V_{ij}$ means repulsive (attractive) interaction. As shown in Fig. 6, $V_{ij}$ values for almost all Fe pairs are negative, so that the attractive interactions are dominant; in particular, the magnitude of the first-nearest-neighbor interaction is significant. Our calculations find that the first-nearest-neighbor Fe pairs gather together with keeping the host Ge crystal structure, i.e., the diamond structure. When the scales of the generated clusters are nanosizes, we call this phenomenon the spinodal nanodecomposition. Note here that this situation is completely different from the (Ge,Mn) case, where many secondary phases precipitate and these crystal structures no longer keep the diamond structure.

In order to clarify the relationship between the inhomogeneity of the doped Fe impurities and magnetic properties, we simulate the formation process of the nanostructure generated by the spinodal nanodecomposition on the basis of the Monte Carlo simulation of the Ising model, $H = -\frac{1}{2}\sum_{i\neq j} V_{ij}\sigma_i\sigma_j$, where $V_{ij}$ is the chemical pair interaction between the Fe pair and $\sigma_i$ is the occupation number (0 or 1) of the

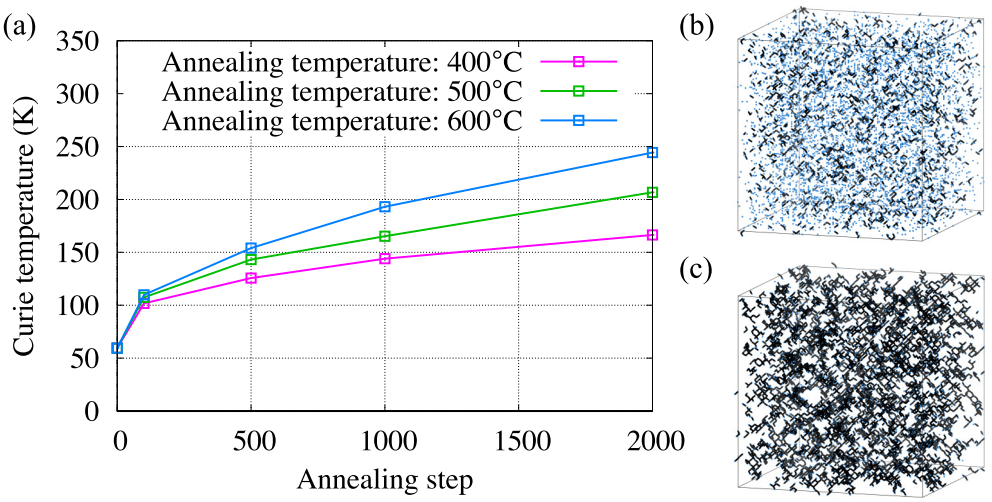


FIG. 7. (Left) (a) Dependence of $T_C$ of $(Ge_{0.895},Fe_{0.105})$ on the annealing steps. The red, green, and blue lines indicate the annealing temperatures by 400, 500, and 600 °C, respectively. (Right) Snapshots of the Monte Carlo simulation for the spinodal nanodecomposition in $(Ge_{0.895},Fe_{0.105})$: (b) initial phase and (c) annealed phase after 2000 Monte Carlo steps. The blue dots and black cylinders indicate the Fe atoms and the first-nearest-neighbor pairs of the Fe atoms, respectively.

Fe atom at site $i$. First, in our simulation, a simulation box with the Ge diamond structure is constructed, and the Fe atoms are randomly distributed in the simulation box. Then, starting from the initial configuration, we simulate an annealing process by the Metropolis algorithm [54]. The results for $(Ge_{0.895},Fe_{0.105})$ are shown in Fig. 7, where Figs. 7(b) and 7(c) correspond to the initial and annealed phases after the 2000 Monte Carlo steps, respectively. We employ the $20 \times 20 \times 20$ conventional diamond structure as the simulation box. The Fe concentrations are fixed to 10.5% and the annealed temperature is 600 °C. Only the Fe atoms are indicated by the blue dots in the figure, and although not shown, the Ge atoms exist in the simulation box. With increasing the annealing steps and proceeding the spinodal nanodecomposition, the Fe atoms construct small nanosize clusters by the attractive interaction between the first-nearest-neighbor pairs (see Fig. 6), indicated by the black cylinders in Fig. 7(c). $T_C$ in the initial phase is considered to be low, because the number of the first-nearest-neighbor Fe-Fe pairs, which have strong ferromagnetic interaction reflecting the double exchange mechanism, is small. When the annealing is proceeded, the magnetic state is drastically changed. Figure 7(a) indicates $T_C$ of the $Ge_{0.895}Fe_{0.105}$ system estimated by the RPA method as a function of the Monte Carlo steps (the annealing steps). The magenta, green, and blue lines correspond to the annealing temperatures of 400, 500, and 600 °C, respectively. As shown in the figure, $T_C$ is also gradually enhanced with proceeding the annealing. This feature can be understood by the fact that the number of the first-neighbor Fe-Fe pairs increases, and at the same time, the magnetic interaction spreads over the whole crystal. Note here that if the nanoclusters are completely isolated, the system becomes a superparamagnetic state; however, actually the nanoclusters interact each other by longer-ranged small ferromagnetic interactions. In particular, the estimated $T_C$ after the 2000 annealing step, in the case of the annealing temperature of 600 °C, is in good agreement with the experimentally observed value. From above discussion, we can conclude that the spinodal nanodecomposition plays an important role to determine the magnetic properties in the Fe-doped Ge system.

## IV. SUMMARY

In this paper, the electronic structures and magnetic properties of the TM-doped Ge, which are IV-type DMS systems, were theoretically investigated by first-principles calculations. Our calculations by KKR Green's function method indicated that the ferromagnetic interactions by the double exchange mechanism are dominant for the Fe- and Co-doped Ge systems. However, these ferromagnetic interactions are quite short ranged compared to the (Ga,Mn)As, and are also weak compared to (Ga,Mn)N, so that we cannot expect high $T_C$ in terms of the magnetic percolation effect if the TM impurities are homogeneously distributed in the hosts. Antiferromagnetic states are stable for the V-, Cr-, and Mn-doped Ge, and the Ni-doped system becomes a nonmagnetic. The inhomogeneity of the TM impurities drastically changes the magnetic states and has a crucial role in the experimentally observed high-$T_C$ ferromagnetism in the IV-type DMSs. The cluster expansion method revealed that the Mn-doped Ge systems tend to generate ordered compounds, such as $Ge_3Mn_5$ and $Ge_8Mn_{11}$, at Mn-rich regions. These precipitated ordered compounds are the causes of the ferromagnetism in (Ge,Mn); in particular $T_C$ of $Ge_3Mn_5$ is consistent with the experimentally observed $T_C$ of (Ge,Mn). The electronic structure of (Ge,Fe) calculated by the VP-SIC method reproduces the spectra of the Fe-3$d$ states in the SX-ARPES experiment. It was proven by the multiscale (scale-bridging) simulations that the Fe atoms are not randomly distributed in the Ge host but gathered with keeping the diamond structure by the attractive pair interactions i.e., the spinodal nanodecomposition. $T_C$ of (Ge,Fe) is enhanced by the annealing process, because the number of the first-nearest-neighbor Fe-Fe pairs with the strong ferromagnetic interaction increases by proceeding

the spinodal nanodecomposition. Our simulations reproduce the experimental magnetic situation very well, and the $T_C$ values estimated by the RPA method are in good agreement with the observed values. We emphasize that the manipulation of structural, configurational, and spin disorders in DMS systems are very important to obtain colossal magnetic responses. In particular, there is the possibility that a drastic magnetic transition between ferromagnetism and antiferromagnetism can be realized in the Ge-doped DMSs by controlling the nanostructure and dimensionality, and applying the gate voltage. Additionally, compared to the typical III-V and II-VI DMSs, the Ge-based DMSs are rather compatible with the present CMOS technology. Utilizing the Ge-based DMSs is a good way to realize next-generation devices based on semiconductor spintronics.

## ACKNOWLEDGMENTS

The authors acknowledge the financial support from JSPS Core-to-Core Program, A. Advanced Research Networks "Computational Nano-materials Design on Green Energy", and Future Research Initiative Group Support Project on "Computational Nano-Materials Design: New Strategic Materials". We acknowledge the financial supports from MEXT KAKENHI (Grants No. 22104012, No. 26286074, and No. 16K21155) and from Japan Science and Technology agency (JST) PREST. T.F. thanks the support from "Building of Consortia for the Development of Human Resources in Science and Technology" and the Supercomputer Center, the Institute for Solid State Physics, the University of Tokyo.

[1] H. Ohno, Science **281**, 951 (1998).
[2] H. Ohno, D. Chiba, F. Matsukura, T. Omiya, E. Abe, and T. Y. O. K. Otani, Nature (London) **408**, 944 (2000).
[3] H. Munekata, H. Ohno, S. von Molnar, A. Segmuller, L. L. Chang, and L. Esaki, Phys. Rev. Lett. **63**, 1849 (1989).
[4] H. Ohno, A. Shen, F. Matsukura, A. Oiwa, A. Endo, S. Katsumoto, and Y. Iye, Appl. Phys. Lett. **69**, 363 (1996).
[5] K. Sato, L. Bergqvist, J. Kudrnovský, P. H. Dederichs, O. Eriksson, I. Turek, B. Sanyal, G. Bouzerar, H. Katayama-Yoshida, V. A. Dinh, T. Fukushima, H. Kizaki, and R. Zeller, Rev. Mod. Phys. **82**, 1633 (2010).
[6] H. Katayama-Yoshida and K. Shindo, Solid State Commun. **44**, 999 (1982).
[7] S. Sonoda, S. Shimizu, T. Sasaki, Y. Yamamoto, and H. Hori, J. Cryst. Growth **237-239**, 1358 (2002).
[8] N. Theodoropoulou, A. F. Hebard, M. E. Overberg, C. R. Abernathy, S. J. Pearton, S. N. G. Chu, and R. G. Wilson, Appl. Phys. Lett. **78**, 3475 (2001).
[9] M. E. Overberg, C. R. Abernathy, S. J. Pearton, N. A. Theodoropoulou, K. T. McCarthy, and A. F. Hebard, Appl. Phys. Lett. **79**, 1312 (2001).
[10] M. L. Reed, N. A. El-Masry, H. H. Stadelmaier, M. K. Ritums, M. J. Reed, C. A. Parker, J. C. Roberts, and S. M. Bedair, Appl. Phys. Lett. **79**, 3473 (2001).
[11] G. T. Thaler, M. E. Overberg, B. Gila, R. Frazier, C. R. Abernathy, S. J. Pearton, J. S. Lee, S. Y. Lee, Y. D. Park, Z. G. Khim, J. Kim, and F. Ren, Appl. Phys. Lett. **80**, 3964 (2002).
[12] K. H. Ploog, S. Dhar, and A. Trampert, J. Vac. Sci. Technol. B **21**, 1756 (2003).
[13] M. Hashimoto, Y.-K. Zhou, M. Kamanura, and H. Asahi, Solid State Commun. **122**, 37 (2003).
[14] L. Gu, S. Y. Wu, H. X. Liu, R. K. Singh, N. Newman, and D. J. Smith, J. Magn. Magn. Mater. **290-291**, 1395 (2003).
[15] K. Sato, W. Schweika, P. H. Dederichs, and H. Katayama-Yoshida, Phys. Rev. B **70**, 201202(R) (2004).
[16] L. Bergqvist, O. Eriksson, J. Kudrnovský, V. Drchal, P. Korzhavyi, and I. Turek, Phys. Rev. Lett. **93**, 137202 (2004).
[17] K. Sato, H. Katayama-Yoshida, and P. H. Dederichs, Jpn. J. Appl. Phys. **44**, L948 (2005).
[18] T. Fukushima, K. Sato, H. Katayama-Yoshida, and P. H. Dederichs, Jpn. J. Appl. Phys. **45**, L416 (2006).
[19] T. Dietl, K. Sato, T. Fukushima, A. Bonanni, M. Jamet, A. Barski, S. Kuroda, M. Tanaka, P. N. Hai, and H. Katayama-Yoshida, Rev. Mod. Phys. **87**, 1311 (2015).
[20] M. Jamet, A. Barski, T. Devillers, V. Poydenot, R. Dujardin, P. Bayle-Guillemaud, J. Rothman, A. M. E. Bellet-Amalric, J. Cibert, R. Mattana, and S. Tatarenko, Nature Mater. **5**, 653 (2006).
[21] T. Devillers, M. Jamet, A. Barski, V. Poydenot, P. Bayle-Guillemaud, E. Bellet-Amalric, S. Cherifi, and J. Cibert, Phys. Rev. B **76**, 205306 (2007).
[22] Y. K. Wakabayashi, Y. Ban, S. Ohya, and M. Tanaka, Phys. Rev. B **90**, 205209 (2014).
[23] S. Sakamoto, Y. K. Wakabayashi, Y. Takeda, S.-i. Fujimori, H. Suzuki, Y. Ban, H. Yamagami, M. Tanaka, S. Ohya, and A. Fujimori, Phys. Rev. B **95**, 075203 (2017).
[24] Y. K. Wakabayashi, S. Sakamoto, Y. Takeda, K. Ishigami, Y. Takahashi, Y. Saitoh, H. Yamagami, A. Fujimori, M. Tanaka, and S. Ohya, Sci. Rep. **6**, 23295 (2016).
[25] P. Hohenberg and W. Kohn, Phys. Rev. **136**, B864 (1964).
[26] W. Kohn and L. J. Sham, Phys. Rev. **140**, A1133 (1965).
[27] J. Korringa, Physica **13**, 392 (1947).
[28] W. Kohn and N. Rostoker, Phy. Rev. **94**, 1111 (1954).
[29] P. Soven, Phys. Rev. B **2**, 4715 (1970).
[30] H. Shiba, Prog. Theor. Phys. **46**, 77 (1971).
[31] Y. K. Wakabayashi, R. Akiyama, Y. Takeda, M. Horio, G. Shibata, S. Sakamoto, Y. Ban, Y. Saitoh, H. Yamagami, A. Fujimori, M. Tanaka, and S. Ohya, Phys. Rev. B **95**, 014417 (2017).
[32] A. Filippetti, C. D. Pemmaraju, S. Sanvito, P. Delugas, D. Puggioni, and V. Fiorentini, Phys. Rev. B **84**, 195127 (2011).
[33] H. Akai, J. Phys.: Condens. Matter **1**, 8045 (1989).
[34] M. Toyoda, H. Akai, K. Sato, and H. Katayama-Yoshida, Phys. Status Solidi **3**, 4155 (2006).
[35] M. Toyoda, H. Akai, K. Sato, and H. Katayama-Yoshida, Physica B **376**, 647 (2006).
[36] A. van de Walle, Calphad **33**, 266 (2009).
[37] A. van de Walle, M. Asta, and G. Ceder, Calphad **26**, 539 (2002).
[38] A. van de Walle and G. Ceder, J. Phase Equilib. **23**, 348 (2002).

[39] G. Kresse and J. Hafner, Phys. Rev. B **47**, 558(R) (1993).
[40] G. Kresse and J. Furthmüller, Phys. Rev. B **54**, 11169 (1996).
[41] G. Kresse and J. Furtfumüller, Comput. Mater. Sci. **6**, 15 (1996).
[42] P. E. Blöchl, Phys. Rev. B **50**, 17953 (1994).
[43] H. J. Monkhorst and J. D. Pack, Phys. Rev. B **13**, 5188 (1976).
[44] A. I. Liechtenstein, M. I. Katsnelson, V. P. Antropov, and V. A. Gubanov, J. Magn. Magn. Mater. **67**, 65 (1987).
[45] A. R. Machintosh and O. K. Andersen, *Electrons at the Fermi Surface* (Cambridge University Press, London, 1980), p. 149.
[46] S. Hilbert and W. Nolting, Phys. Rev. B **70**, 165203 (2004).
[47] G. Bouzerar, T. Ziman, and J. Kudrnovský, Europhys. Lett. **69**, 812 (2005).
[48] F. Ducastelle and F. Gautier, J. Phys. F **6**, 2039 (1976).
[49] L. Chen, S. Yan, P. F. Xu, J. Lu, W. Z. Wang, J. J. Deng, X. Qian, Y. Ji, and J. H. Zhao, Appl. Phys. Lett. **95**, 182505 (2009).
[50] L. Chen, X. Yang, F. Yang, J. Zhao, J. Misuraca, P. Xiong, and S. von Molnár, Nano Lett. **11**, 2584 (2011).
[51] R. I. Andrusyak and B. Y. Kotur, Russ. Metall. **4**, 204 (1991).
[52] J. P. Perdew and A. Zunger, Phys. Rev. B **23**, 5048 (1981).
[53] See Supplemental Material at http://link.aps.org/supplemental/10.1103/PhysRevB.96.104415 for the comprehensive comparison with the LDA.
[54] N. Mertopolis, A. W. Rosenbluth, M. N. Rosenbluth, and A. H. Teller, J. Chem. Phys. **21**, 1087 (1953).